Spectroscopic fingerprints of many-body renormalization in $1T$-$TiSe_2$

J. Zhao,[1] Kyungmin Lee,[2] J. Li,[1] D. B. Lioi,[3] G. Karapetrov,[3] Nandini Trivedi,[2] and U. Chatterjee[1,*]

[1]*Department of Physics, University of Virginia, Charlottesville, Virginia 22904, USA*

[2]*Department of Physics, The Ohio State University, Columbus, Ohio 43210, USA*

[3]*Department of Physics, Drexel University, Philadelphia, Pennsylvania 19104, USA*

(Received 20 December 2018; published 8 July 2019)

We have investigated many-body renormalizations of the single-particle excitations in $1T$-$TiSe_2$ by employing high resolution angle-resolved photoemission spectroscopy (ARPES) measurements. The energy distribution curves (EDCs) of the ARPES data reveal an intrinsic single band peak-dip-hump (PDH) feature. Furthermore, the renormalized electronic dispersion extracted from the momentum distribution curves (MDCs) highlights a well-defined kink structure. These are canonical signatures of many-body correlations in the system. Theoretical modeling of the electrons coupled to an Einstein mode illustrates that a study of the renormalized dispersion from the MDCs enable direct access to the characteristic features of these many-body correlations, such as the energy scale of the relevant collective mode and the strength of its coupling with the electrons in the system. This model also demonstrates the difficulty to determine these features in a straightforward way from the PDH structure of the EDCs. The self-energy analysis of our ARPES data suggest compelling evidence for a bosonic mode having energy $\sim$26 meV, with which the electrons in $1T$-$TiSe_2$ couple to. This correlates with the *ab initio* phonon-dispersion calculations and the observation of breathing (A_{1g}) phonon mode in Raman scattering experiments.

DOI: 10.1103/PhysRevB.100.045106

I. INTRODUCTION

The origin of various emergent phenomena in quantum materials, such as superconductivity in cuprate and pnictide high temperature superconductors [1–3], unusual mass renormalization in heavy fermion compounds [4,5], and colossal magnetoresistance in manganites [6,7] arise from many-body interactions involving only electrons, and/or electrons and some collective mode in the system. In the physics of many of these phenomena, bosonic modes—such as phonons, spin fluctuations, and magnons—play a crucial role, either acting as the intermediary "glue" between electrons, or as the modes that condense upon phase transition. Therefore, an in-depth study of the electron-boson coupling is pivotal to explore the microscopic mechanism and their manifestations of such quantum phenomena.

$1T$-$TiSe_2$, a widely studied TMD material, is composed of van der Waals coupled Se-Ti-Se trilayers [Fig. 1(a)], that undergoes a second-order phase transition from a semimetal/semiconductor [8–11] to a commensurate CDW state below the transition temperature ($T_{CDW} \sim 200$ K) [12]. It has been found that T_{CDW} of $1T$-$TiSe_2$ can be suppressed to zero either by chemical intercalation [13,14], or by strain engineering [15]. In both cases, superconductivity emerges in a dome-shaped region of the corresponding phase diagram, reminiscent of HTSCs [1–3] and heavy fermion compounds [4,5].

Despite elaborate research, the mechanisms of the CDW order in pristine $1T$-$TiSe_2$ and superconductivity in Cu-intercalated $1T$-$TiSe_2$ are controversial. In general, a long-range CDW order in a system is accompanied by the softening of a bosonic mode coupled to the electrons. It is, however, not straightforward to disentangle the precise nature of the bosonic mode in case of $1T$-$TiSe_2$. This mode could be (a) purely electronic in origin, known as the so-called exciton that is a bound state of an electron and a hole, with the CDW formation described by a Bose-Einstein condensation of excitons below T_{CDW} [16,17] or (b) phononic in origin, in which case the CDW formation is related to a Jahn-Teller-like lattice distortion occurring via strong electron-phonon interactions in the system [18–20].

Previously, several ARPES measurements have been interpreted using the excitonic condensation model [21–26]. Moreover, the recently developed technique of momentum-resolved electron energy-loss spectroscopy (M-EELS) has provided evidence for the softening of a bosonic mode with predominantly electronic character [27]. On the other hand, a number of scanning tunneling microscopy studies [28,29] and ultrafast spectroscopic measurements [30] suggest the role of a local structural instability due to electron-phonon interactions in driving the CDW order in $1T$-$TiSe_2$.

There are indeed several comprehensive theoretical works on various aspects of phonons in $1T$-$TiSe_2$. For instance, Motizuki and coworkers [31–33] developed a general picture of lattice distortions in TMDs including $1T$-$TiSe_2$. Recent first-principles calculations [34] reported that the CDW transition in pristine $1T$-$TiSe_2$ and the emergence of superconductivity in pressurized $1T$-$TiSe_2$ samples can be entirely ascribed to electron-phonon interactions. Additionally, the role of electron-phonon interactions has been emphasized [35] for fully explaining the so-called chiral nature of the CDW

*uc5j@virginia.edu

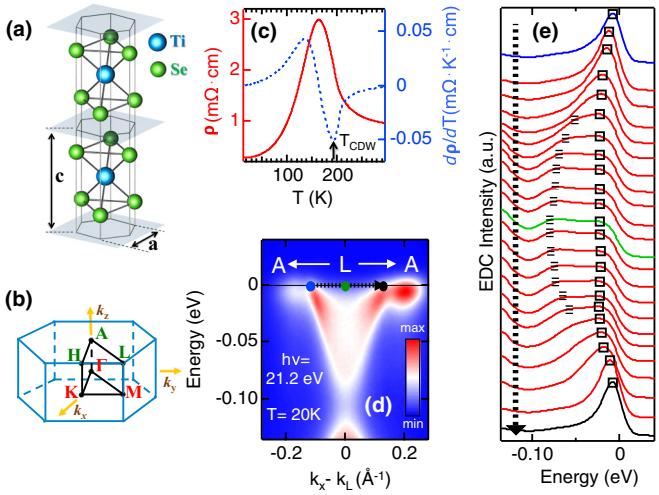

FIG. 1. Peak-dip-hump structure of the ARPES data. (a) Schematic crystal structure and (b) Brillouin zone of the normal state of $1T$-$TiSe_2$; the high-symmetry points are marked. (c) Plots of the in-plane resistivity ρ vs T (red curve) and $\frac{d\rho}{dT}$ vs T (blue dashed curve). T_{CDW} is determined from the minimum (pointed by the black arrow) of $\frac{d\rho}{dT}$ vs T plot. (d) The energy-momentum intensity map (EMIM) of the conduction band around the L point. (e) Energy distribution curves (EDCs) along the trajectory between two Fermi momenta marked by the black (k_F) and blue ($-k_F$) dots in (d). These EDCs are offset for visual clarity. Peak-dip-hump (PDH) structure of these EDCs are clearly visible. Peaks are shown by the open squares, while the humps are shown by the dashed lines. The ARPES data, shown in this figure, were recorded with $h\nu = 21.2$ eV at 20 K.

state in $1T$-$TiSe_2$. On the experimental front, the phonon density of states and phonon softening have been probed by x-ray [36–39] and Raman scattering experiments [40,41].

There are also two conflicting views on the superconducting glue in Cu-doped $1T$-$TiSe_2$ samples. The first one relies on the competition between superconducting and CDW order, and suggests that superconductivity is stabilized by fluctuations of the CDW order above a certain critical concentration of the Cu atoms that leads to the disappearance of CDW order [13,42]. According to the second hypothesis, a combination of enhanced electron-phonon coupling and increased density of states at the chemical potential gives rise to superconductivity in samples with high concentration of Cu atoms [34,43]. In this picture, the competition between superconducting and CDW order in the phase diagram of Cu-doped $1T$-$TiSe_2$ samples is purely coincidental. Given all these, a direct investigation of electron-phonon coupling in $1T$-$TiSe_2$ is highly desirable.

A straightforward way to examine how a bosonic mode impacts the electronic excitations of a solid is to focus on the momentum and energy dependence of the single particle spectral function $A(\mathbf{k},\omega) = (-1/\pi)\mathrm{Im}G(\mathbf{k},\omega)$ [44], that is directly measured by ARPES and calculated from the retarded Green's function G. The self-energy $\Sigma(\mathbf{k},\omega)$ that describes the effect of many-body renormalization of a single-particle spectrum, is a complex-valued function whose real part contains information about the renormalization of the bare electronic dispersion, while the imaginary part represents the lifetime-broadening because of interactions. Thus the direct effect of electron-boson interaction is contained in the self energy, through renormalizations of various attributes of an electron, such as its mass, charge, and quasiparticle weight. As, for instance, the direct signature of electron-boson coupling in ARPES is the appearance of a kink feature in the renormalized band dispersion. The origin of such a kink can be understood as follows: the dispersion close to the chemical potential becomes flatter due to an enhancement in the effective mass of the quasiparticles, while the dispersion sufficiently away from the chemical potential practically follows the bare dispersion. It is possible to gain valuable information on the electron-boson coupling of a system from the analysis of its dispersion kinks. A large body of work has been devoted to the examinations of the dispersion anomalies in different TMDs [45–50]. Strikingly, such a study on $1T$-$TiSe_2$ is lacking. This motivates our present self-energy analysis of the ARPES data from $1T$-$TiSe_2$.

Our main results are the following: We detected a pronounced kink structure in the electronic dispersion of $1T$-$TiSe_2$. The self-energy analysis of the ARPES data backed by theoretical calculations enable us to conclude an electron-boson coupling being the origin of this kink structure. Finally, a comparison to the first-principles calculations of vibrational properties and Raman scattering data suggest that this boson in all likelihood is the breathing (A_{1g}) phonon mode of the system. However, we could not detect electron-boson coupling at the ~50 meV energy, referred as the signature of the excitonic mode in recent M-EELS [27] studies.

II. EXPERIMENTAL DETAILS

We conducted ARPES measurements on $1T$-$TiSe_2$ single crystals using 21.2 eV Helium-I line of a discharge lamp combined with a Scienta R3000 analyzer at the University of Virginia, as well as 24 and 43 eV synchrotron light equipped with a Scienta R4000 electron analyzer at the SIS beamline of the Swiss Light Source, Paul Scherrer Institute, Switzerland. The energy and momentum resolutions were approximately 8–20 meV and 0.0055 $Å^{-1}$ respectively. Single crystals were cleaved *in situ* to expose a fresh surface of the crystal for ARPES measurements. Samples were cooled using a closed cycle He refrigerator and the sample temperatures were monitored using a silicon diode sensor mounted close to the sample holder. During each measurement, the chemical potential μ of the system was determined by analyzing ARPES data from a polycrystalline gold sample in electrical contact with the sample of interest. High quality single crystals of $1T$-$TiSe_2$ were grown using the standard iodine vapor transport method and the samples were characterized using x-ray diffraction, energy dispersive x-ray spectroscopy (EDS), and electrical resistivity measurements. Raman scattering measurements were performed at the Center for Nanoscale Materials at Argonne National Laboratory, using the Renishaw In Via Raman microscope with a 514 nm argon ion laser source and a ~1.5 μm diameter spot size. This Raman spectrometer is equipped with variable temperature cell using which temperature-dependent measurements can be conducted between 80 and 500 K.

III. RESULTS

A. Intrinsic PDH structure of the energy distribution curves

We start with a schematic layout of the normal state three-dimensional Brillouin zone of $1T$-$TiSe_2$ in Fig. 1(b), which marks the high-symmetry points. $T_{CDW} \sim 200$ K is determined from the measurement of the in-plane electrical resistivity ρ as a function of temperature T in Fig. 1(c).

The electronic structure above T_{CDW} consists of a valence band centered at the Γ point mainly composed of Se $4p$ states separated by a small gap from the conduction band located at the L point predominantly composed of $3d$ states of Ti. To elucidate various attributes of the many-body interactions, we focus on the line shape analysis of the ARPES EDCs. In Fig. 1(e), we present a sequence of EDCs at 20 K, associated with an ARPES energy-momentum intensity map (EMIM) around the L point as shown in Fig. 1(d). The EMIM depicts the ARPES intensity as a function of one of the in-plane momentum components and electronic energy ($\overline{\omega}$) referenced to the chemical potential μ, while keeping the other orthogonal in-plane momentum component fixed. The EDCs in Fig. 1(e) are located at equidistant momenta along the trajectory between two Fermi momenta (k_F and $-k_F$) as shown by the black and blue dots on the EMIM in Fig. 1(d). These EDCs clearly display two-peak features, commonly referred to as the PDH structure [51–54]. An earlier ARPES study [55] also reported two-peak structure of EDCs in $1T$-$TiSe_2$.

Typically, an intrinsic PDH structure of the EDCs associated with a single energy band is an indicative of a nontrivial many-body interaction, such as the coupling of electrons to a bosonic mode in the system [56,57]. In the presence of such a coupling, the spectral weight gets split into two parts: (i) a relatively sharp quasiparticle peak with a shallow dispersion at low energies, and (ii) a "hump"-like broad and incoherent feature in the spectrum at higher energies.

To examine whether the above-described PDH structure is an intrinsic attribute of a single-band, we analyze photon energy ($h\nu$) dependence of the ARPES data in Fig. 2. The EMIM in Fig. 1(d) is recorded with an incident photon energy $h\nu = 21.2$ eV. We add to that data using two other EMIMs in Figs. 2(a) ($h\nu = 24$ eV) and 2(b) ($h\nu = 43$ eV). The EDCs constructed from Figs. 2(a) and 2(b) are displayed in Figs. 2(c) and 2(d), respectively. The PDH structure of the EDCs are noticeable in the data recorded with all three photon energies. This leads us to conclude that the PDH structure of the EDC's in the current case is inherent. We also checked that the variations of the intensities of the peaks and humps of the EDCs at equivalent momenta scale together reasonably well with changing $h\nu$. These observations imply that the intensities of both the peak and hump features are governed by common matrix elements, which further evidence the intrinsic nature of the PDH structure of the EDCs. From the above-described observations, we infer that the PDH line shape of $1T$-$TiSe_2$ indeed carries the signature of many-body correlations in the system. It is worthwhile to point out that the characteristic features of the many-body phenomenon such as the energy scale of the collective mode and/or coupling strength cannot be directly estimated from the PDH structure itself. We illustrate this difficulty through an explicit model calculation of the spectral function in Sec. III B.

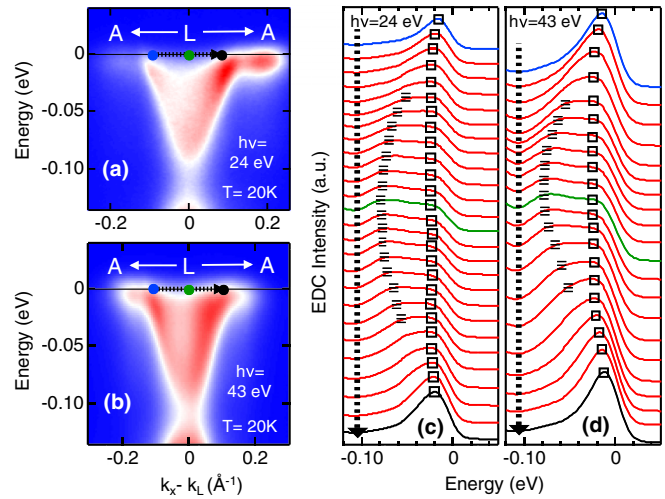

FIG. 2. ARPES data with different incident photon energies. EMIMs, similar to that in Fig. 1(d), are displayed in (a) and (b) with $h\nu = 24$ and 43 eV, respectively. The sequence of EDCs corresponding to (a) and (b) are shown in (c) and (d), respectively. The PDH structure of the EDCs is visible in (c) and (d) like in Fig. 1(c).

B. Modeling of the PDH structure by coupling electrons to an Einstein mode

For comparison with the ARPES data and to gain insight into their features, we calculated the spectral function $A(\mathbf{k}, \overline{\omega})$ of electrons coupled to an Einstein mode of energy Ω. The single-particle self-energy $\Sigma(\mathbf{k}, \overline{\omega})$ represents the electron-boson coupling in the Born-Oppenheimer approximation is given by

$$\Sigma(\mathbf{k}, \overline{\omega}) = \int d\omega' d^d q \; g_{\mathbf{q}}^2 G^{(0)}(\mathbf{k}-\mathbf{q}, \overline{\omega}-\omega') D^{(0)}(\mathbf{q}, \omega'), \quad (1)$$

where $G^{(0)}$ and $D^{(0)}$ are the propagators of the noninteracting electron and the bosonic mode, respectively. For simplicity, we adopt the approximation of constant lifetime above and below $\pm\Omega$ away from the Fermi level [58], where the self-energy is written as

$$\Sigma(\overline{\omega}) = \alpha_f \frac{\epsilon_F}{\pi} \log\left(\frac{\Omega - \overline{\omega} - i\eta}{\Omega + \overline{\omega} + i\eta}\right) \equiv \alpha_f \epsilon_F \Sigma(\overline{\omega}), \quad (2)$$

where ϵ_F is the Fermi energy of the noninteracting electron band, α_f is a dimensionless coupling strength, and η is the intrinsic broadening. $\Sigma(\overline{\omega}$ is the (dimensionless) normalized self-energy that is taken to be momentum-independent. The single-particle spectral function $A(\mathbf{k}, \overline{\omega})$ can be expressed in terms of the electronic self-energy as follows:

$$A(\mathbf{k}, \overline{\omega}) = \frac{-\Sigma''(\overline{\omega})}{(\overline{\omega} - \epsilon_{\mathbf{k}} - \Sigma'(\overline{\omega}))^2 + \Sigma''(\overline{\omega})^2}. \quad (3)$$

Here $\epsilon_{\mathbf{k}}$ represents the noninteracting band dispersion, while $\Sigma'(\overline{\omega})$ and $\Sigma''(\overline{\omega})$ correspond to real and imaginary parts of the self-energy, respectively. As to the further details of the calculation of $A(\mathbf{k}, \overline{\omega})$, (i) we assumed a quadratic dispersion $\epsilon_{\mathbf{k}}/\epsilon_F = (k/k_F)^2 - 1$, and (ii) the values of the mode energy Ω, and intrinsic broadening η of the spectral function are taken to be $\Omega/\epsilon_F = 0.25$ and $\eta/\epsilon_F = 0.1$, respectively. The dimensionless coupling constant α_f for Figs. 2(a) and 2(b) is taken to be $\alpha_f = 0.5$.

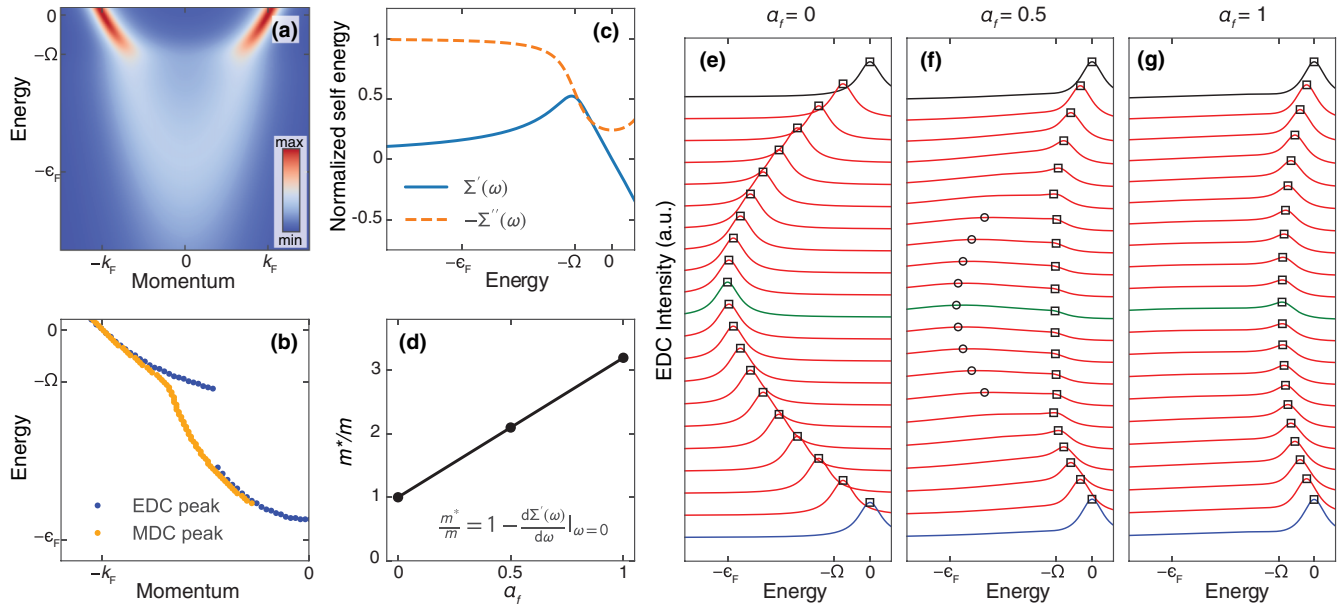

FIG. 3. Results from a model calculation. (a) Intensity map of the calculated single-particle spectral function $A(\mathbf{k}, \overline{\omega})$. (b) Dispersions extracted from the calculated $A(\mathbf{k}, \overline{\omega})$. Blue and yellow markers represent the dispersions obtained by tracking the peaks of the EDCs and MDCs, respectively. MDC-derived dispersion clearly exhibits a kink, whose $\overline{\omega}$ location coincides with the mode energy Ω. EDC-derived dispersion, on the other hand, shows a two-branched behavior—the upper branch corresponds to the dispersion of the quasiparticle peak and the lower branch to that of the hump. (c) Real part Σ' and imaginary part Σ'' of (dimensionless) normalized self energy as functions of $\overline{\omega}$. (d) Mass renormalization as a function of the coupling strength between the electrons and the bosonic mode. (e–g) EDCs at several momenta, which are equispaced and located between $-k_F$ and k_F, for (e) $\alpha_f = 0$, (f) $\alpha_f = 0.5$, and (g) $\alpha_f = 1$. Blue and black curves in (e-f) represent the EDCs at $-k_F$ and k_F, respectively. The green curves mark the EDCs located at the band bottom, i.e., at $k = 0$. Black squares denote the locations of the "peaks" of the EDCs in the energy window: $-2\Omega \leqslant \overline{\omega} \leqslant 0$, while the black circles point the positions of the humps as defined by the local maxima of the EDCs in the energy range $\overline{\omega} \leqslant -\Omega$.

A clear kink structure is visible in the electronic dispersion, derived from the MDC's, shown in Fig. 3(b). The energy location of the kink matches nicely with the mode energy. As expected, the dispersion derived from the EDCs has two branches: the top branch with narrow dispersion is related to the sharp quasiparticle peak, while the bottom branch concerns with the broad hump feature and it essentially tracks the noninteracting dispersion away from the mode energy.

In Fig. 3(c), we show the forms of the normalized self-energy $\Sigma'(\overline{\omega})$ and $\Sigma''(\overline{\omega})$ used for the calculation. It is important to mention that for $-\Omega < \overline{\omega} < \Omega$, $\Sigma''(\overline{\omega})$ should be identically zero due to the fact that the scattering process described by Eq. (1) becomes purely virtual. This is indeed the case for Eq. (2) in the limit $\eta \to 0^+$. However, Σ'' in Fig. 3(c) remains nonzero because of the finite value of η. In this context, the values of η, α_f and Ω have been chosen in such a way that the characteristic features of the calculated $A(\mathbf{k}, \overline{\omega})$ best describes the data.

While the imaginary part Σ'' of self-energy provides (energy-dependent) broadening to the spectral function, the real part Σ' alters its dispersion. Bosonic mode coupling leads to a shallower electronic dispersion near the Fermi level, as can be seen in Figs. 3(a) and 3(b). The effect is captured by the increase in the effective mass m^* (or equivalently, decrease in the Fermi velocity v_F^*) as

$$\frac{m^*}{m} = \frac{v_F^0}{v_F^*} = 1 - \left.\frac{d\Sigma'(\overline{\omega})}{d\overline{\omega}}\right|_{\overline{\omega}=0}, \tag{4}$$

where m and v_F^0 are the bare mass and the bare Fermi velocity, respectively. Figure 3(d) shows m^* as a function of coupling strength α_f. Within the choice of α_f we used in the calculation, the mass enhancement ranges up to $\sim$3 times.

The EDCs associated with the calculated $A(\mathbf{k}, \overline{\omega})$ are shown in Figs. 3(e) to 3(g), for $\alpha_f = 0$ (bare dispersion), $\alpha_f = 0.5$ [same as in Figs. 3(a) and 3(b)], and $\alpha_f = 1$, respectively. The EDCs with intermediate coupling strength, shown in Fig. 3(f), are able to capture the essential PDH features in the experimental EDC data shown in Figs. 1(e), 2(c), and 2(d). The EDCs clearly show spectral shift from $\epsilon_{\mathbf{k}}$ to $-\Omega$ with increasing coupling strength.

We would like to point out that our purpose here was not to conduct a full-fledged modeling of the ARPES data; rather, the aim was to capture some of the essential features of the data by invoking a simple model. Our simple theoretical model provides the following important insights. (i) Even though the effect of an electron-mode coupling can be observed in the EDCs, it is not straightforward to detect the energy scale of the mode from the EDCs. (ii) The energy scale(s) of the mode, on the other hand, can be determined from the energy scale of the kink of the dispersion derived from the MDCs. Based on these understandings, we conduct an analysis of the momentum distribution curves (MDCs) of the ARPES data in Sec. III C for directly extracting the energy scale(s) of the mode.

C. Kink structure in the electronic dispersion

The relationship between ARPES intensity $I(\mathbf{k},\overline{\omega})$ and single-particle spectral function $A(\mathbf{k},\overline{\omega})$ is approximately given by $I(\mathbf{k},\overline{\omega}) \sim M(\mathbf{k})A(\mathbf{k},\overline{\omega})f(\overline{\omega})$, where (i) $f(\overline{\omega})$ is the Fermi-Dirac distribution function, (ii) $M(\mathbf{k})$ is the dipole matrix element. As shown by Eq. (3), $A(\mathbf{k},\overline{\omega})$ can be expressed in terms of Σ'' and Σ'. The self-energy analysis from the data, however, becomes tractable only when Σ is independent of $\mathbf{k}$ or is weakly $\mathbf{k}$-dependent. Quite generally, for a relatively small value of $|\overline{\omega}|$, the MDC takes a simple Lorentzian line shape provided Σ is $\mathbf{k}$-independent. This is because $\epsilon_{\mathbf{k}}$ in the vicinity of k_F can be linearized as follows: $\epsilon_{\mathbf{k}} \sim v_F^*(|\mathbf{k}| - k_F)$ with v_F^* being the renormalized Fermi velocity [51–54]. The renormalized dispersion of an energy band can be determined by plotting the fitted peak positions of the corresponding MDCs at different values of $\overline{\omega}$. The deviation of this renormalized dispersion from the bare dispersion provides a measure for $\Sigma'(\overline{\omega})$ [51–54]. Additionally, $\Sigma''(\overline{\omega})$ can be quantified from the fitted peak widths $W(\overline{\omega})$ of the MDCs. The relation between $\Sigma''(\overline{\omega})$ and $W(\overline{\omega})$ is as follows: $W(\overline{\omega}) = \frac{\Sigma''(\overline{\omega})}{v_F^*}$ [51–54].

Figure 4(a) presents the experimental MDCs for several values of $\overline{\omega}$ along the trajectory marked by the black dashed arrow in the EMIM in Fig. 1(d). In Fig. 4(b), we superimpose the dispersion curve on the second derivative of this EMIM with $\overline{\omega}$. A quick glance at Fig. 4(b) reveals a clearly identifiable kink, i.e., a change in slope, of the renormalized electronic dispersion, for $\overline{\omega} \sim -26$ meV. It seems that there are also features at smaller values of $|\overline{\omega}|$ (marked by dotted circles in Fig. 4(c)), which are, however, difficult to resolve.

It is worth mentioning that kink features in the electronic dispersion have also been observed in a wide variety of solid state systems, including various $2H$-polytypes of TMDs [45–50], metallic systems [59,60], conventional superconductors [61], manganites [62], cuprate high temperature superconductors [51–54], and pnictide high temperature superconductors [63].

D. Identity of the bosonic mode

It was already pointed out that the presence of a kink in the electronic dispersion is typically construed as a fingerprint of electronic scattering from a bosonic mode [44,52,53]. To address the identity of the mode in the present case, we turn our attention to the self-energy analysis of the ARPES data. The knowledge of the bare band dispersion is necessary for evaluating $\Sigma'(\overline{\omega})$ from the data. This is approximated by a straight line, which follows the high binding energy part of the MDC-derived dispersion and also passes through k_F. Similar approximation has been adopted for other systems, too [47,52–54,61–63]. We quantify $\Sigma'(\overline{\omega})$ by subtracting the approximated bare band dispersion from the measured one. Additionally, $\Sigma''(\overline{\omega})$ is obtained from $W(\overline{\omega})$. $\Sigma'(\overline{\omega})$ and $W(\overline{\omega})$ are plotted in Figs. 4(c) and 4(d), respectively. An unambiguous peaky feature of $\Sigma'(\overline{\omega})$ for $\overline{\omega} \sim -26$ meV can easily be deciphered from Fig. 4(c). This energy scale agrees well with that of the Raman active breathing (A_{1g}) phonon mode as can be seen in our Raman data in Fig. 4(e). Various phonon modes as well as CDW amplitude modes in our Raman data are consistent with previous measurements [40,64–67]. There are also additional structures of $\Sigma'(\overline{\omega})$ and $\Sigma''(\overline{\omega})$ for smaller values of $|\overline{\omega}|$, which are hard to decode and have been indicated by dotted circles in Fig. 4.

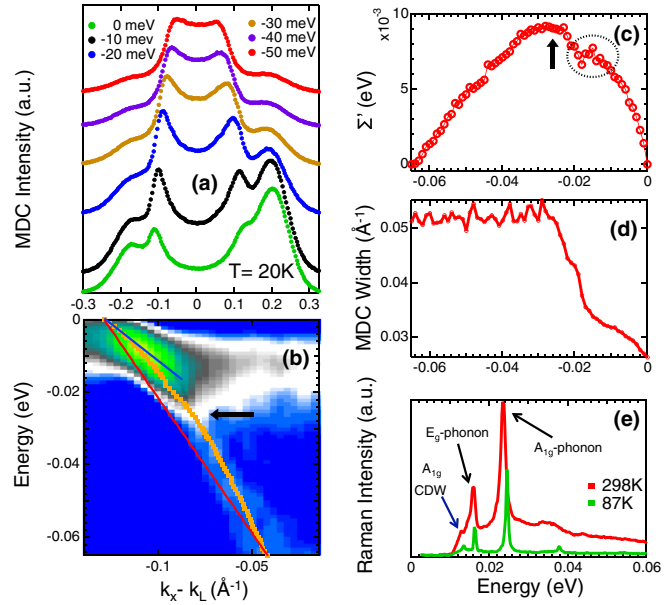

FIG. 4. Self-energy analysis of ARPES data. (a) MDCs for a series $\overline{\omega}$'s along the momentum line, shown by the black dashed arrow in Fig. 1(d). These MDCs are offset for visual clarity. Renormalized band dispersion (orange markers) from MDC analysis is superimposed on the second derivative of the energy-momentum intensity map of Fig. 1(d) with respect $\overline{\omega}$ in (b). Approximated bare band dispersion is shown by the red line, whose slope determines v_F^0. The slope of the blue line, which corresponds to the slope of the renormalized dispersion at $\overline{\omega} = 0$, determines v_F^*. A Kink structure at $\overline{\omega} \sim -26$ meV can easily be discerned from the renormalized dispersion. $\Sigma'(\overline{\omega})$ and $W(\overline{\omega})$ are displayed in (c) and (d), respectively. Black arrow in (c) points the peaky structure of $\Sigma'(\overline{\omega})$ at $\overline{\omega} \sim -26$ meV. From (b), (c), and (d), it can be seen that the $\overline{\omega}$ location of the black arrows approximately matches with the $\overline{\omega}$, at which the slope of $W(\overline{\omega})$ changes. Note that $\Sigma'(\overline{\omega})$ is directly proportional to $W(\overline{\omega})$. The black dotted circles mark the features in the dispersion as well as in $\Sigma'(\overline{\omega})$ for $|\overline{\omega}| < 26$ meV. These features are not clearly resolved and they can be related to the shear phonon mode and/or the CDW amplitude modes. Here, we show the data corresponding to the left branch of the intensity map. We check that the right branch also gives similar result. (e) Temperature evolution of Raman spectra of $1T$-$TiSe_2$ single crystal. Raman data display energy scales of the A_{1g} CDW amplitude mode, and breathing (A_{1g}) and shear (E_g) phonon modes.

These low-energy features could, in principle, be related to the E_g phonon mode and/or the CDW amplitude modes. Based on the data presented in Fig. 4, it would be natural to conclude that the electron-phonon coupling is responsible for the renormalization of the electronic dispersion of $1T$-$TiSe_2$. It is worth mentioning that kink structures of phononic origin have also been reported in ARPES studies of other TMDs, such as $2H$-$NbSe_2$ [46,47] and $2H$-TaS_2 [50].

It was already pointed out that the PDH structure of the EDCs of $1T$-$TiSe_2$ was also observed in a previous ARPES study [55]. Moreover, this work reported a strong temperature dependence of the PDH structure—with increasing temperature, the PDH structure becomes weak and eventually

vanishes. Our MDC analysis, as elaborated above, provides convincing arguments for electron-phonon interactions being one of the drivers behind many-body renormalizations in $1T$-$TiSe_2$. It is worth noting that these two results do not necessarily contradict with each other. This is because (i) as detailed in Sec. III B, the characteristic energy scales of the collective mode, whose coupling to the electrons gives rise to the PDH structure, are not directly related to those of the PDH feature and (ii) the occupied band-width of the $3d$ electron pocket in $1T$-$TiSe_2$ is known to decrease with increasing temperature [20,68,69] which can take into account of the gradual weakening and eventual disappearance of the PDH structure as temperature is increased.

E. Estimate of electrical resistivity using Drude model

To correlate our MDC analysis with the electrical transport measurements of the system, we estimate electrical resistivity ρ using the Drude model $\rho = \frac{m^*}{ne^2\tau}$, where m^* is the effective mass of the charge carriers, n is the carrier density, and τ is the scattering lifetime. We find $n \sim 10^{20}\,\mathrm{cm}^{-3}$ from our Hall measurements. The other two Drude parameters, τ and m^*, are approximated from the MDC analysis [70]. The scattering lifetime $\tau \sim \frac{\hbar}{\Sigma''(\tilde{\omega}=0)} \sim 23\,\mathrm{fs}$ and the effective mass $m^* \sim (1+\lambda)m_e$, where λ is the mass enhancement due to many-body interactions and m_e is the bare electronic mass. To be precise, we should have used band-mass m_{LDA} instead of m_e in the previous expression for m^*. Given that m_{LDA} is not expected to be significantly different from m^* and since we are aiming for only an order of magnitude estimate for ρ, we use m_e. From Fig. 4(b), we find that $v_F^* = 0.54\,\mathrm{eV}\cdot$ Å and $v_F^0 = 0.78\,\mathrm{eV}\cdot$ Å Combining the parameters above, we find $\rho \sim 2.24\,\mathrm{m}\Omega\cdot\mathrm{cm}$, which is in reasonable agreement with the experimentally measured value of $\rho \sim 0.4\,\mathrm{m}\Omega\cdot\mathrm{cm}$ [Fig. 1(c)].

IV. CONCLUSION

In summary, we report here the first observation of a pronounced dispersion-anomaly due to many-body effect in the ARPES spectra of $1T$-$TiSe_2$ around the L point. From a self-energy analysis of our data, and combining with Raman scattering, we find that the Raman active breathing (A_{1g}) phonon mode is one of the main collective modes in the system, with which the electrons couple to. We, however, cannot rule out the possibility of the coupling with the shear phonon mode and/or the CDW amplitude modes. Future studies with laser-based ARPES at very low temperatures would be useful to render further insights into these modes. The direct observation of a kink feature in ARPES experiment and its agreement with the theoretical modeling of electrons coupled to a bosonic mode suggest the potential relevance of electron-phonon interactions to the origin of the CDW and superconducting orders in compounds based on $1T$-$TiSe_2$.

ACKNOWLEDGMENTS

U.C., J.Z., J.L. acknowledge support from the National Science Foundation (NSF) under Grant No. DMR-1629237. N.T. and K.L. acknowledge support from the National Science Foundation (NSF) under Grant No. DMR-1629382. G.K. acknowledges the support by the National Science Foundation under Grant No. ECCS-1711015. U.C. also acknowledges support from the Jefferson Trust at the university of Virginia for the ARPES instrumentation at his laboratory. The use of the Center for Nanoscale Materials, an Office of Science user facility, was supported by the US Department of Energy, Office of Science, Office of Basic Energy Sciences, under Contract No. DE-AC02-06CH11357.

[1] J. G. Bednorz and K. A. Müller, Z. Phys. **64**, 189 (1986).
[2] P. A. Lee, N. Nagaosa, and X. G. Wen, Rev. Mod. Phys. **78**, 17 (2006).
[3] J. Orenstein and A. J. Millis, Science **288**, 468 (2000).
[4] *Theory of Heavy Fermions and Valence Fluctuations*, edited by T. Kasuya and T. Saso, Proceedings of the Eighth Taniguchi Symposium (Springer, New York, 1985).
[5] P. Gegenwart, Q. Si, and F. Steglich, Nat. Phys. **4**, 186 (2008).
[6] M. B. Salamon and M. Jaime, Rev. Mod. Phys. **73**, 583 (2001).
[7] E. Dagotto, New J. Phys. **7**, 67 (2005).
[8] G. Li, W. Z. Hu, D. Qian, D. Hsieh, M. Z. Hasan, E. Morosan, R. J. Cava, and N. L. Wang, Phys. Rev. Lett. **99**, 027404 (2007).
[9] J. Wilson, Solid State Commun. **22**, 551 (1977).
[10] T. E. Kidd, T. Miller, M. Y. Chou, and T.-C. Chiang, Phys. Rev. Lett. **88**, 226402 (2002).
[11] J. C. E. Rasch, T. Stemmler, B. Müller, L. Dudy, and R. Manzke, Phys. Rev. Lett. **101**, 237602 (2008).
[12] F. Di Salvo, D. Moncton, and J. Waszczak, Phys. Rev. B **14**, 4321 (1976).
[13] E. Morosan, H. W. Zandbergen, B. S. Dennis, J. W. G. Bos, Y. Onose, T. Klimczuk, A. P. Ramirez, N. P. Ong, and R. J. Cava, Nat. Phys. **2**, 544 (2006).
[14] E. Morosan, K. E. Wagner, Liang L. Zhao, Y. Hor, A. J. Williams, J. Tao, Y. Zhu, and R. J. Cava, Phys. Rev. B **81**, 094524 (2010).
[15] A. F. Kusmartseva, B. Sipos, H. Berger, L. Forró, and E. Tutiš, Phys. Rev. Lett. **103**, 236401 (2009).
[16] A. N. Kozlov and L. A. Maksimov, Sov. Phys. JETP **21**, 790 (1965).
[17] L. V. Keldysh and Y. V. Kopaev, Sov. Phys. Solid State **6**, 2219 (1965).
[18] H. Hughes, J. Phys. C **10**, L319 (1977).
[19] M. Whangbo and E. Canadell, J. Am. Chem. Soc. **114**, 9587 (1992).
[20] A. Wegner, J. Zhao, J. Li, J. Yang, A. A. Anikin, G. Karapetrov, D. Louca, and U. Chatterjee, arXiv:1807.05664.
[21] H. Cercellier, C. Monney, F. Clerc, C. Battaglia, L. Despont, M. G. Garnier, H. Beck, P. Aebi, L. Patthey, H. Berger, and L. Forró, Phys. Rev. Lett. **99**, 146403 (2007).
[22] C. Monney, H. Cercellier, F. Clerc, C. Battaglia, E. F. Schwier, C. Didiot, M. G. Garnier, H. Beck, P. Aebi, H. Berger, L. Forró, and L. Patthey, Phys. Rev. B **79**, 045116 (2009).
[23] C. Monney, H. Cercellier, F. Clerc, C. Battaglia, E. Schwier, C. Didiot, M. Garnier, H. Beck, and P. Aebi, Physica B (Amsterdam) **404**, 3172 (2009).

[24] C. Monney, G. Monney, P. Aebi, and H. Beck, Phys. Rev. B **85**, 235150 (2012).

[25] C. Monney, G. Monney, P. Aebi, and H. Beck, New J. Phys. **14**, 075026 (2012).

[26] C. Monney, C. Battaglia, H. Cercellier, P. Aebi, and H. Beck, Phys. Rev. Lett. **106**, 106404 (2011).

[27] A. Kogar, M. S. Rak, S. Vig, A. A. Husain, F. Flicker, Y. Il Joe, L. Venema, G. J. MacDougall, T. C. Chiang, E. Fradkin, J. van Wezel, and P. Abbamonte, Science **358**, 1314 (2017).

[28] B. Hildebrand, T. Jaouen, C. Didiot, E. Razzoli, G. Monney, M.-L. Mottas, A. Ubaldini, H. Berger, C. Barreteau, H. Beck, D. R. Bowler, and P. Aebi, Phys. Rev. B **93**, 125140 (2016).

[29] B. Hildebrand, T. Jaouen, C. Didiot, E. Razzoli, G. Monney, M.-L. Mottas, F. Vanini, C. Barreteau, A. Ubaldini, E. Giannini, H. Berger, D. R. Bowler, and P. Aebi, Phys. Rev. B **95**, 081104(R) (2017).

[30] M. Porer, U. Leierseder, J.-M. Ménard, H. Dachraoui, L. Mouchliadis, I. E. Perakis, U. Heinzmann, J. Demsar, K. Rossnagel, and R. Huber, Nat. Mater. **13**, 857 (2014).

[31] Y. Yoshida and K. Motizuki, J. Phys. Soc. Jpn. **49**, 898 (1980).

[32] N. Suzuki, A. Yamamoto, and K. Motizuki, J. Phys. Soc. Jpn. **54**, 4668 (1985).

[33] N. Suzuki, H. Yoshiyama, K. Motizuki, and Y. Takaoka, Synth. Met. **19**, 887 (1987).

[34] M. Calandra and F. Mauri, Phys. Rev. Lett. **106**, 196406 (2011).

[35] B. Zenker, H. Fehske, H. Beck, C. Monney, and A. R. Bishop, Phys. Rev. B **88**, 075138 (2013).

[36] A. Kogar, G. A. de la Pena, S. Lee, Y. Fang, S. X.-L. Sun, D. B. Lioi, G. Karapetrov, K. D. Finkelstein, J. P. C. Ruff, P. Abbamonte, and S. Rosenkranz, Phys. Rev. Lett. **118**, 027002 (2017).

[37] M. Holt, P. Zschack, Ha. Hong, M. Y. Chou, and T.-C. Chiang, Phys. Rev. Lett. **86**, 3799 (2001).

[38] F. Weber, S. Rosenkranz, J.-P. Castellan, R. Osborn, G. Karapetrov, R. Hott, R. Heid, K.-P. Bohnen, and A. Alatas, Phys. Rev. Lett. **107**, 266401 (2011).

[39] M. Maschek, S. Rosenkranz, R. Hott, R. Heid, M. Merz, D. A. Zocco, A. H. Said, A. Alatas, G. Karapetrov, S. Zhu, J. van Wezel, and F. Weber, Phys. Rev. B **94**, 214507 (2016).

[40] C. S. Snow, J. F. Karpus, S. L. Cooper, T. E. Kidd, and T.-C. Chiang, Phys. Rev. Lett. **91**, 136402 (2003).

[41] H. Barath, M. Kim, J. F. Karpus, S. L. Cooper, P. Abbamonte, E. Fradkin, E. Morosan, and R. J. Cava, Phys. Rev. Lett. **100**, 106402 (2008).

[42] D. Qian, D. Hsieh, L. Wray, E. Morosan, N. L. Wang, Y. Xia, R. J. Cava, and M. Z. Hasan, Phys. Rev. Lett. **98**, 117007 (2007).

[43] J. F. Zhao, H. W. Ou, G. Wu, B. P. Xie, Y. Zhang, D. W. Shen, J. Wei, L. X. Yang, J. K. Dong, M. Arita, H. Namatame, M. Taniguchi, X. H. Chen, and D. L. Feng, Phys. Rev. Lett. **99**, 146401 (2007).

[44] J. Bardeen, L. N. Cooper, and J. R. Schrieffer, Phys. Rev. **106**, 162 (1957).

[45] T. Valla, A. V. Fedorov, P. D. Johnson, J. Xue, K. E. Smith, and F. J. DiSalvo, Phys. Rev. Lett. **85**, 4759 (2000).

[46] T. Valla, A. V. Fedorov, P. D. Johnson, P.-A. Glans, C. McGuinness, K. E. Smith, E. Y. Andrei, and H. Berger, Phys. Rev. Lett. **92**, 086401 (2004).

[47] D. J. Rahn, S. Hellmann, M. Kalläne, C. Sohrt, T. K. Kim, L. Kipp, and K. Rossnagel, Phys. Rev. B **85**, 224532 (2012).

[48] K. Rossnagel, Eli Rotenberg, H. Koh, N. V. Smith, and L. Kipp, Phys. Rev. B **72**, 121103(R) (2005).

[49] J. Zhao, K. Wijayaratne, A. Butler, J. Yang, C. D. Malliakas, D. Y. Chung, D. Louca, M. G. Kanatzidis, J. van Wezel, and U. Chatterjee, Phys. Rev. B **96**, 125103 (2017).

[50] K. Wijayaratne, J. Zhao, C. Malliakas, D. Y. Chung, M. G. Kanatzidis, and U. Chatterjee, J. Mater. Chem. C **5**, 11310 (2017).

[51] S. Hüfner, *Photoelectron Spectroscopy: Principles and Applications* (Springer, New York, 2003).

[52] J. C. Campuzano, M. R. Norman, and M. Randeria, in *Physics of Superconductors*, edited by K. H. Bennemann and J. B. Ketterson (Springer, Berlin, 2004), Vol. 2, pp. 167–273.

[53] A. Damascelli, Z. Hussain, and Z. X. Shen, Rev. Mod. Phys. **75**, 473 (2003).

[54] P. D. Johnson, A. V. Fedorov, and T. Valla, J. Electron Spectrosc. Relat. Phenom. **117–118**, 153 (2001).

[55] C. Monney, E. F. Schwier, M. G. Garnier, C. Battaglia, N. Mariotti, C. Didiot, H. Cercellier, J. Marcus, H. Berger, A. N. Titov, H. Beck, and P. Aebi, Europhys. Lett. **92**, 47003 (2010).

[56] M. R. Norman and H. Ding, Phys. Rev. B **57**, R11089(R) (1998).

[57] S. Engelsberg and J. R. Schrieffer, Phys. Rev. **131**, 993 (1963).

[58] G. D. Mahan, *Many-Particle Physics* (Springer, New York, 2000).

[59] T. Valla, A. V. Fedorov, P. D. Johnson, and S. L. Hulbert, Phys. Rev. Lett. **83**, 2085 (1999).

[60] Ph. Hofmann, I. Yu. Sklyadneva, E. D. L. Rienks, and E. V. Chulkov, New J. Phys. **11**, 125005 (2009).

[61] D. Mou, R. Jiang, V. Taufour, R. Flint, S. L. Bud'ko, P. C. Canfield, J. S. Wen, Z. J. Xu, G. Gu, and A. Kaminski, Phys. Rev. B **91**, 140502(R) (2015).

[62] Z. Sun, Y.-D. Chuang, A. V. Fedorov, J. F. Douglas, D. Reznik, F. Weber, N. Aliouane, D. N. Argyriou, H. Zheng, J. F. Mitchell, T. Kimura, Y. Tokura, A. Revcolevschi, and D. S. Dessau, Phys. Rev. Lett. **97**, 056401 (2006).

[63] L. Wray, D. Qian, D. Hsieh, Y. Xia, L. Li, J. G. Checkelsky, A. Pasupathy, K. K. Gomes, C. V. Parker, A. V. Fedorov, G. F. Chen, J. L. Luo, A. Yazdani, N. P. Ong, N. L. Wang, and M. Z. Hasan, Phys. Rev. B **78**, 184508 (2008).

[64] S. Sugai, K. Murase, S. Uchida, and S. Tanaka, Solid State Commun. **35**, 433 (1980).

[65] J. V. Yakhmi, I. K. Gopalakrishnan, L. C. Gupta, A. M. Umarji, R. Vijayaraghavan, and R. M. Iyer, Phys. Rev. B **35**, 7122 (1987).

[66] D. L. Duong, G. Ryu, A. Hoyer, C. Lin, M. Burghard, and K. Kern, ACS Nano **11**, 1034 (2017).

[67] L. Cui, R. He, G. Li, Y. Zhang, Y. You, and M. Huang, Solid State Commun. **266**, 21 (2017).

[68] C. Monney, E. F. Schwier, M. G. Garnier, N. Mariotti, C. Didiot, H. Beck, P. Aebi, H. Cercellier, J. Marcus, C. Battaglia, H. Berger, and A. N. Titov, Phys. Rev. B **81**, 155104 (2010).

[69] Th. Pillo, J. Hayoz, H. Berger, F. Lèvy, L. Schlapbach, and P. Aebi, Phys. Rev. B **61**, 16213 (2000).

[70] T. Yoshidaa, X. J. Zhou, H. Yagi, D. H. Lu, K. Tanaka, A. Fujimori, Z. Hussain, Z.-X. Shen, T. Kakeshitad, H. Eisaki S. Uchida, Kouji Segawa, A. N. Lavrov, and Y. Ando, Physica B (Amsterdam) **351**, 250 (2004).